# Dynamic Analysis Tool for Moored Tanker-Based FPSO's including Large Yaw Motions

by
M.H. Kim, Associate Professor
Department of Civil Engineering, Texas A&M University

**Final Project Report Prepared for the Minerals Management Service**
**Under the MMS/OTRC Cooperative Research Agreement**
**1435-01-99-CA-31003**
**Task Order 16181**
**Project 366**

**and**

**OTRC Industry Consortium**

**November 2004**

OTRC Library Number: 11-04/A144



*For more information contact:*

**Offshore Technology Research Center**
Texas A&M University
1200 Mariner Drive
College Station, Texas 77845-3400
(979) 845-6000

or

**Offshore Technology Research Center**
The University of Texas at Austin
1 University Station C3700
Austin, Texas 78712-0318
(512) 471-6989

*A National Science Foundation Graduated Engineering Research Center*

# Dynamic Analysis Tool for Moored Tanker-Based FPSO's including Large Yaw Motions

## Abstract

A vessel/mooring/riser coupled dynamic analysis program in time domain is developed for the global motion simulation of a turret-moored, tanker based FPSO designed for 6000-ft water depth. The vessel and line dynamics are solved simultaneously in a combined matrix for the given environmental and boundary conditions. The vessel global motions and mooring tension are tested at the OTRC wave basin for the non-parallel wind-wave-current 100-year hurricane condition in the Gulf of Mexico. The same case is also numerically simulated using the developed coupled dynamic analysis program. The numerical results are compared with the OTRC 1:60 model-testing results with truncated mooring system.

The system's stiffness and line tension as well as natural periods and damping obtained from the OTRC measurement reasonably match with numerically simulated static-offset and free-decay tests. The numerically predicted global vessel motions are also in good agreement with the measurements. It is underscored that the dynamic mooring tension can be underestimated when truncated mooring system is used.

## Introduction

FPSOs have been successfully installed and operated around the world during the past decade and many new FPSOs will be designed and installed in the coming years. In particular, with increasing interest in their use in the Gulf of Mexico, model tests were conducted at the Offshore Technology Research Center (OTRC) multi-directional wave basin to examine the behavior of generic FPSOs in wave, wind, and current conditions typical of the passage of severe hurricane (Ward et al, 2001). FPSOs for the Gulf of Mexico will likely be passively moored through a turret system so that the tanker can weathervane or rotate in response to the changing wave, wind, and current directions in a hurricane. The waves, winds, and currents can be quite non-parallel, and subject the vessel to quartering or beam seas that can significantly influence the response of a ship-shaped vessel.

Several researchers have studied the dynamic characteristics of FPSOs in winds, waves, and currents. Wichers (1988), for example, initiated a comprehensive study for numerical simulations of a turret-moored FPSO in irregular waves with winds and currents. He derived the equation of motions of such model in the time domain using an uncoupled method and solved rigid-body and mooring-line dynamics separately. Other researchers (Sphaier et al., 2000, Lee and Choi, 2000) investigated the behavior and stability of turret-moored FPSOs based on a set of simplified ship-maneuvering equations.

In this study, FPSO responses in hurricane seas predicted by a vessel-mooring-riser coupled dynamic analysis program were compared to wave tank measurements. A tanker-based turret-moored FPSO moored by a 12 chain-polyester-chain taut lines in 6,000 ft of water was studied. A series of model tests (1:60 scale) were conducted in the Offshore Technology Research Center's wave basin at Texas A&M University with statically-equivalent truncated mooring system to assess its performance in the hurricane condition. Since the water depth is large, it is expected that a significant portion of the total damping comes from the long slender members and they may also contribute appreciably to the system's total stiffness and inertia. The mismatch of Reynolds numbers between the slender members of model and the prototype is another generic problem in the physical model testing. Therefore, for the reasonable assessment of the role of slender members on vessel motions, the hull/mooring/riser coupled dynamic analysis is essential.

The dynamic interactions between hull and slender members can be evaluated numerically in several ways. One simple approach is called uncoupled analysis, which assumes that mooring lines and risers respond statically (as a mass-less nonlinear spring) to hull motions (e.g. Lee and Choi, 2000). With this assumption, the inertia effects and hydrodynamic loading on mooring lines and risers are neglected. After hull motions are calculated, the mooring and riser dynamics can be evaluated independently by inputting the fairlead responses. The reliability and accuracy of this approach is expected to diminish as water depth increases. Kim et al.(2001b) and Ma & Lee (2000) showed that such uncoupled analysis of TLPs and spars may be inaccurate when used in deepwater. Wichers et al. (2001a and 200b) also showed that the uncoupled analysis may give even larger error in case of FPSO. Wichers et al. (2001a and 2001b) concluded that fully coupled dynamic models are necessary to estimate realistic design values. Using hull/mooring/riser coupled dynamic analysis tools, the effects of risers and mooring lines on FPSO hull motions and vice versa can be more accurately predicted.

## Description of the System and Experiments

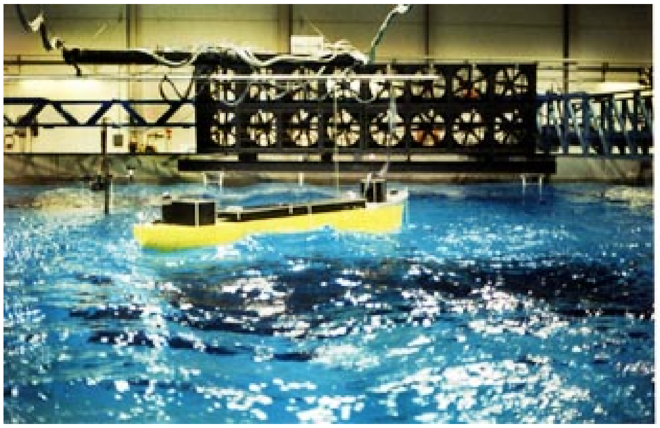

**Figure 1.** OTRC wave basin and FPSO model

The FPSO hull and mooring system used in this study were very similar to those of the fully-loaded 6000ft-FPSO used in the DeepStar study (e.g. Wichers and Devlin, 2001 and 2004; Kim and Kim, 2002). Details of the OTRC FPSO experiments were published by Ward et al (2001 and 2004).

The turret location was changed to a more forward position (38.73-m or 12.5% of Lpp aft of the forward perpendicular) and vessel draft changed from 18.9m to 15.12 m to reflect an 80 % loading condition. The OTRC wave basin and FPSO model are shown in Figure 1. The corresponding vessel displacement is calculated to be 186,051 MT. The details of the FPSO particulars are shown in Table 1. The general arrangement and body plan of the vessel are shown in Figure 2. As shown in the figure, the vessel bow is toward the East (the bow is heading the East).

The mooring lines were hinged to and spread from the turret. The prototype system had 12 mooring lines consisting of chain, polyester, and chain. There are 4 groups of lines, each group consists of 3 lines 5-degrees apart. Each mooring line has a studless chain anchor of Grade K4. Table 2 shows the main particulars of prototype mooring lines. Table 3 gives the hydrodynamic coefficients for the mooring lines. The effects of tangential drag and tangential added inertia of mooring lines and Coulomb friction from seabed were expected to be unimportant, and thus they were not included.

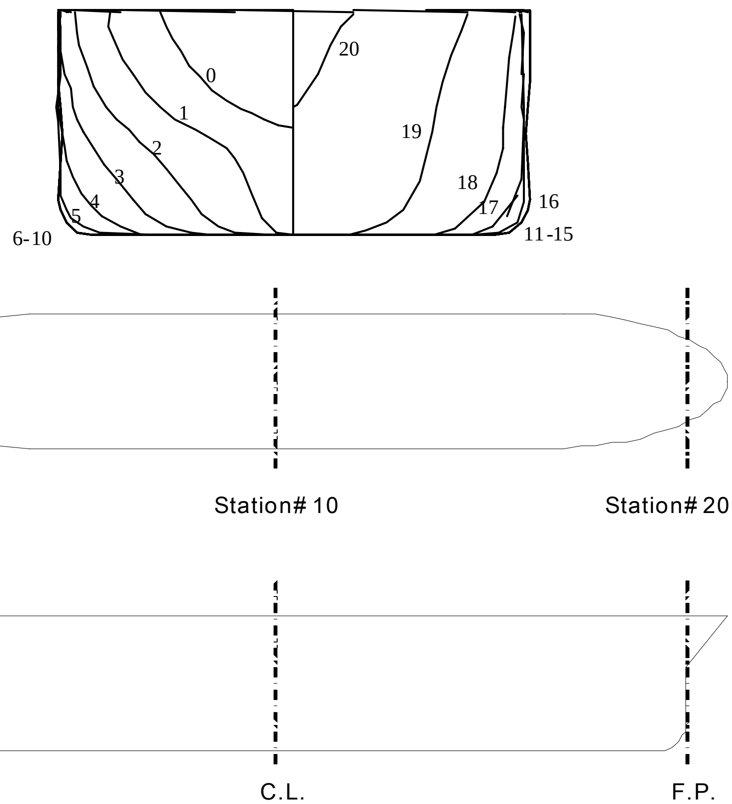


**Figure 2.** General arrangement and body plan of FPSO 6,000 ft.

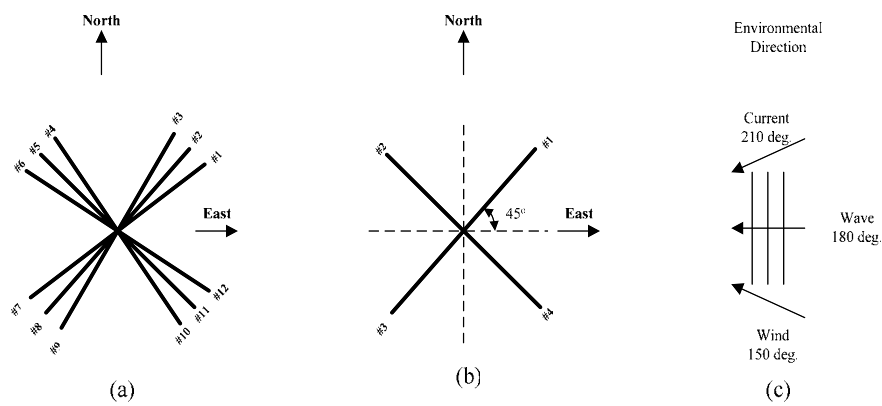


**Figure 3.** Arrangement of mooring lines for turret-moored FPSO:
(a) Mooring system of the prototype FPSO (12-line mooring), (b) Mooring system of the OTRC experiment (4-equivalent mooring), (c) Wave, wind, & current directions

Four equivalent mooring lines were used, with each equivalent line representing the combined effects of 3 mooring lines. The equivalent diameter was derived from the condition of 'equal drag force'. Figure 3 shows the prototype (a) and equivalent mooring systems (b). The mooring system was rotated 90 degrees from that used in the DeepStar study.

In the 1:60-scale OTRC experiment, the water depth cannot be proportionally scaled (a tank depth of 100 feet would be required). Therefore, an equivalent mooring system was developed using steel wires, springs, clumps weights, and buoys to represent the static surge stiffness of the prototype mooring design as closely as possible. Due to its complexity, the direct numerical modeling of the truncated mooring system was not attempted. The total length of the truncated mooring used in the experiment was 43ft (2580 ft at prototype scale), while the actual length would have been 145 ft (8700 ft at prototype scale).

Instrumentation on the FPSO measured the 6DOF motions, accelerations at the turret location, and mooring top tensions. Probes located at six reference positions in the basin measured the wind, wave, and current conditions.

**Table 1.** Main particulars of the turret-moored FPSO used for the OTRC experiment

| **Description** | **Symbol** | **Unit** | **Quantities** |
|---|---|---|---|
| Production level | | *bpd* | 120,000 |
| Storage | | *bbls* | 1,440,000 |
| Vessel size | | *kDWT* | 200.0 |
| Length between perpendicular | Lpp | *m* | 310.00 |
| Breadth | B | *m* | 47.17 |
| Depth | H | *m* | 28.04 |
| Draft (in 80% loaded) | T | *m* | 15.121 |
| Displacement (in 80% loaded)[1)] | | *MT* | 186,051 |
| Length-beam ratio | L/B | | 6.6 |
| Beam-draft ratio | B/T | | 3.12 |
| Block coefficient | Cb | | 0.85 |
| Center of buoyancy[1)] (origin: turret) | $x_b$ | *m* | -108.67 |
| | $z_b$ | *m* | -7.30 |
| Center of gravity (origin: turret) | $x_g$ | *m* | -109.67 |
| | $z_g$ | *m* | -1.8 |
| Water plane area[1)] | A | $m^2$ | 12,927 |
| Frontal wind area | Af | $m^2$ | 4209.6 |
| Transverse wind area | Ab | $m^2$ | 16018.6 |
| Roll radius of gyration at CG | $R_{xx}$ | *m* | 14.036 |
| at Turret | $R_{xx}$ | *m* | 14.151 |
| Pitch radius of gyration at CG | $R_{yy}$ | *m* | 77.47 |
| at Turret | $R_{yy}$ | *m* | 134.28 |
| Yaw radius of gyration CG | $R_{zz}$ | *m* | 79.30 |
| at Turret | $R_{zz}$ | *m* | 135.34 |
| Turret in center line behind Fpp (12.5% Lpp) | Xtur | *m* | 38.73 |
| Turret elevation below tanker base | Ztur | *m* | 1.52 |
| Turret Diameter | | *m* | 15.85 |

Remark: 1) The quantities are obtained from WAMIT

**Table 2.** Main particulars of mooring systems for the OTRC FPSO

| Designation | Unit | Quantity |
|---|---|---|
| Water depth | *m* | 1829 |
| Pre-tension | *kN* | 1424 |
| Number of lines | | 4×3 |
| Degree between the 3 lines | *deg.* | 5 |
| Length of mooring line | *m* | 2652 |
| Radius of location of chain stoppers on turn table | *m* | 7.0 |
| Segment 1(ground section): Chain | | |
| Length at anchor point | *m* | 121.9 |
| Diameter | *cm* | 9.52 |
| Dry weight | *N/m* | 1856 |
| Weight in water | *N/m* | 1615 |
| Stiffness AE | *kN* | 820900 |
| Mean breaking load (MBL) | *kN* | 7553 |
| Segment 2: Polyester Rope | | |
| Length | *m* | 2438 |
| Diameter | *cm* | 16.0 |
| Dry weight | *N/m* | 168.7 |
| Weight in water | *N/m* | 44.1 |
| Stiffness AE | *kN* | 168120 |
| Mean breaking load (MBL) | *kN* | 7429 |
| Segment 1(ground section): Chain | | |
| Length at anchor point | *m* | 91.4 |
| Diameter | *cm* | 9.53 |
| Dry weight | *N/m* | 1856 |
| Weight in water | *N/m* | 1615 |
| Stiffness AE | *kN* | 820900 |
| Mean breaking load (MBL) | *kN* | 7553 |

**Table 3.** Hydrodynamic coefficients of the chain, rope and wire for the OTRC FPSO (Tangential drag and added inertia and Coulomb friction over seabed are ignored)

| Hydrodynamic Coefficients | Symbol | Chain | Rope/Poly |
|---|---|---|---|
| Normal drag | $C_{dn}$ | 2.45 | 1.2 |
| Normal added inertia coefficient | $C_{in}$ | 2.00 | 1.15 |

***Environmental Data***

For experiments and simulations, the 100-year hurricane condition for the Gulf of Mexico (GoM) were similar to those used in the DeepStar study. The wave condition is given by JONSWAP spectrum with a significant wave height of 12 m, a peak period of 14 sec, and a peak enhancement factor of 2.5. To generate wind loading, the NPD wind spectrum was used, which is shown in Figure 4. The mean wind velocity at the reference height of 10 m for one hour was 41.12 m/s.

The storm current velocity near free surface is 0.91m/s. For the intermediate region between 60.96 m to 91.44 m, the current profile is varied linearly. The summary of the environmental conditions for this study is shown in Table 4.

The wind/current force coefficients for the present 80% loading condition were linearly interpolated from the two sets (full and ballast loading) of OCIMF curves.

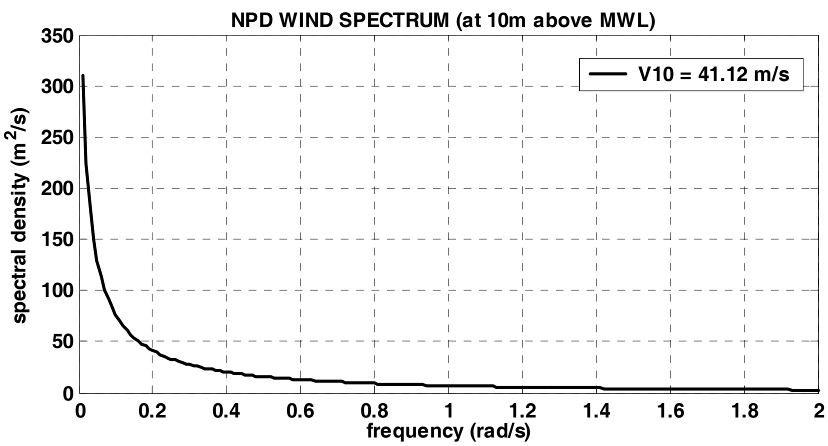


**Figure 4.** NPD wind spectrum (at 10m above MWL, V10 = 41.12m/s)

**Table 4.** Environmental loading condition for the OTRC FPSO

| Description | Unit | Quantities |
|---|---|---|
| **Wave** | | |
| Significant wave height, Hs | *m* | 12.19 |
| Peak periods, Tp | *sec* | 14 |
| Wave spectrum | JONSWAP (GAMMA = 2.5) | |
| Direction | *deg* | 180[1)] |
| **Wind** | | |
| Velocity at 10m above MWL | *m/s* | 41.12 |
| Spectrum | NPD | |
| Direction | *deg* | 150[1)] |
| **Current** | | |
| Profile | | |
| at free surface 0m | *m/s* | 0.9144 |
| at 60.96m | *m/s* | 0.9144 |
| at 91.44m | *m/s* | 0.0914 |
| on the sea bottom | *m/s* | 0.0914 |
| Direction | | 210[1)] |

Remark: 1) The angle is measured counterclockwise from the x-axis (the East).

# Numerical Modeling

### *Hull Hydrodynamics*

The design data $L \times B \times D$, $T$, $KG$, the turret position, and the top tension of mooring lines etc. are taken from Ward et al. (2001). In the same paper, natural frequencies and damping coefficients measured from a series of free decay tests are also given. The added mass and radiation damping, first-order wave-frequency forces, and second-order mean and difference-frequency forces were calculated from the 3D second-order diffraction/radiation panel program WAMIT (Lee, 1999). Figure 5 shows the distribution of panels on the body surface.

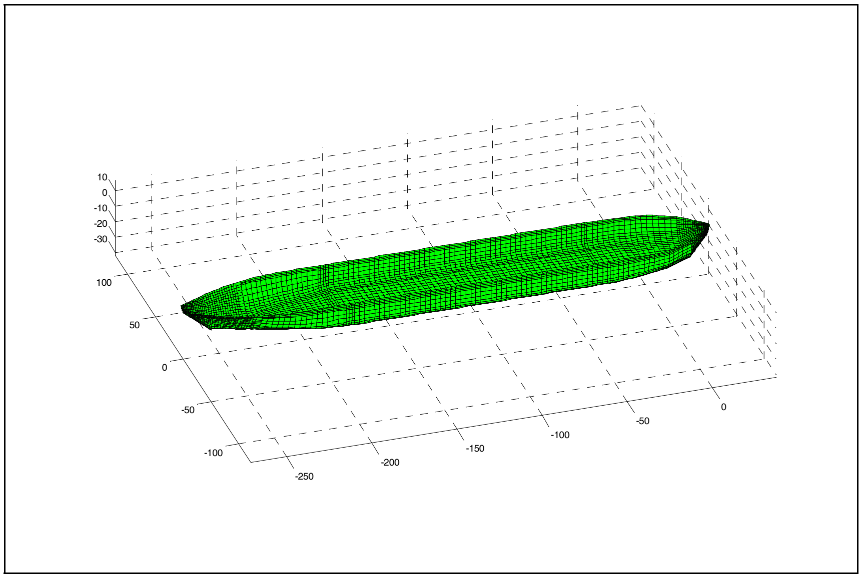


**Figure 5.** Mesh generation of the turret-moored FPSO

Taking advantage of symmetry, only half domain is discretized (2448 panels for hull). All the hydrodynamic coefficients were calculated in the frequency domain, and then the corresponding forces were converted to the time domain using two-term Volterra series expansion. The phase shift of incident waves due to slow drift motions was also considered. The frequency-dependent radiation damping was included in the form of convolution integral in the time domain equation. The wave drift damping was calculated from Aranha's formula and found to be small, and thus not included in the ensuing analysis (Arcandra, 2001).

The methodology for hull/mooring/riser coupled statics/dynamics is similar to that of Kim & Kim (2002). The mooring lines are assumed hinged at the turret and anchor position. The wave force quadratic transfer functions are computed for 9 wave frequencies, ranging from 0.24 to 1.8 rad/sec and the intermediate values for other frequencies are interpolated. The hydrodynamic coefficients and wave forces are expected to vary appreciably with large yaw angles and the effects should be taken into consideration for the reliable prediction of FPSO global motions. Therefore, they are calculated in advance for various yaw angles with 5-degree interval and the data are then tabulated as inputs (Arcandra et al, 2002).

The second-order diffraction/radiation computation for a 3D body is computationally very intensive especially when it has to be run for various yaw angles. Therefore, many researchers have avoided such a complex procedure by using a simpler approach called Newman's approximation. The off-diagonal components of the second-order difference-frequency QTFs are approximated by their diagonal values (mean drift forces and moments). The approximation can be justified when the system's natural frequency is very small and the slope of QTFs near the diagonal is not large. In Kim (2003) the validity of Newman's approximation is tested to be reasonable against more accurate results with complete QTFs.

From the WAMIT output, the water-plane area, the displacement volume, the center of buoyancy and the restoring coefficients were obtained. Based on these data, the vertical static equilibrium of the FPSO can be checked i.e. the sum of the vertical line top tensions and the weight is to be equal to the buoyancy. The relations between the natural frequency, and the restoring coefficients/masses are defined as follows:

$$f = \frac{1}{2\pi}\sqrt{\frac{C_{ij}}{M_{Vij}}} \text{ (1/sec or Hz)} \quad (i, j = 1, 2, \cdots, 6) \tag{1}$$

where $f$ is the natural frequency, $C_{ij}$ is the restoring coefficients (hydrostatic + mooring), and $M_{V\,ij}(= M_{aij} + m_{ij})$ is the virtual mass in which $M_{aij}$ is the added mass near natural frequencies and $m_{ij}$ is the mass/inertia of the body. From the WAMIT output, $M_{V\,ij}$ can be obtained.

**Slender Member Dynamics**

For the static/dynamic analysis of mooring lines and risers, an extension of the theory developed for slender rods by Garrett (1982) was used. Assuming that there is no torque or twisting moment, one can derive a linear momentum conservation equation with respect to a position vector $\vec{r}(s,t)$ which is a function of arc length $s$ and time $t$ :

$$-(B\vec{r}'')'' + (\lambda\vec{r}')' + \vec{q} = m\ddot{\vec{r}} \tag{2}$$

$$\lambda = T - B\kappa^2 \tag{3}$$

where primes and dots denote spatial s-derivative and time derivative, respectively, $B$ is the bending stiffness, $T$ the local effective tension, $\kappa$ the local curvature, $m$ the mass per unit length, and $\vec{q}$ the distributed force on the rod per unit length. The scalar variable $\lambda$ can be regarded as a Lagrange multiplier. The rod is assumed to be elastic and extensible, thus the following condition is applied

$$\frac{1}{2}(\vec{r}\cdot\vec{r} - 1) = \frac{T}{A_t E} \approx \frac{\lambda}{A_t E} \tag{4}$$

where E=Young's modulus, $A_t = A_e - A_i$ (=outer – inner cross sectional area). For these equations, geometric non-linearity is fully considered and there is no special assumption made concerning the shape or orientation of lines. The benefit of this equation is that (2) is directly defined in the global coordinate system and does not require any transformations to the local coordinate system, which saves overall computational time significantly.

The normal component of the distributed external force on the rod per unit length, $q_n$, is given by a generalized Morison equation:

$$q_n = C_I \rho A_e \dot{v}_n + C_D \frac{1}{2}\rho D |v_{nr}| v_{nr} + C_m \rho A_e \ddot{r}_n \tag{5}$$

where $C_I, C_D$ and $C_m$ are inertia, drag, and added mass coefficients, and $\dot{v}_n, v_{nr}$, and $\ddot{r}_n$ are normal fluid acceleration, normal relative velocity, and normal structure acceleration, respectively. The symbols $\rho$ and $D$ are fluid density and local diameter. In addition, the effective weight, or net buoyancy, of the rod should be included in $q_n$ as a static load.

A finite element method similar to Garrett (1982) has been developed to solve the above mooring dynamics problem and the details of the methodology are given in Ran et al. (1997) and Ran (2000). The FEM allows any combination of mooring types and materials as long as their deformations are small and within proportional limit. The upper ends of the mooring lines and risers are connected to the hull fairlead through generalized elastic springs and dampers. The combination of linear and torsional springs can model arbitrary connection conditions. The forces and moments proportional to the relative displacements are transmitted to the hull at the connection points. The transmitted forces from mooring lines and risers to the platform are given by

$$\tilde{F}_P = \tilde{K}(\tilde{T}\tilde{u}_P - \tilde{u}_I) + \tilde{C}(\tilde{T}\dot{\tilde{u}}_P - \dot{\tilde{u}}_I), \tag{6}$$

where $\tilde{K}, \tilde{C}$ are stiffness and damping matrices of mooring lines at the connection point, and $\tilde{T}$ represents a transformation matrix between the platform origin and connection point. The symbols $\tilde{u}_P, \tilde{u}_I$ represent column matrices for the displacements of the platform and connection point.

Then, the following hull response equation can be combined into the riser/mooring-line equations in the time domain:

$$\begin{aligned}(\tilde{M} + \tilde{M}_a(\infty))\ddot{\tilde{u}}_p + \int_0^\infty \tilde{R}(t-\tau)\dot{\tilde{u}}_p d\tau + \tilde{K}_H \tilde{u}_p = \\ \tilde{F}_D + \tilde{F}^{(1)} + \tilde{F}^{(2)} + \tilde{F}_p + \tilde{F}_w + \tilde{F}_c + \tilde{F}_{WD}\end{aligned} \tag{7}$$

where $\tilde{M}, \tilde{M}_a$ are mass and added mass matrix, $\tilde{R}$ =retardation function (inverse cosine Fourier transform of radiation damping) matrix, $\tilde{K}_H$ =hydrostatic restoring coefficient, $\tilde{F}_D$ =drag force matrix on the hull, $\tilde{F}^{(1)}, \tilde{F}^{(2)}$ =first- and second-order wave load matrix on the hull, $\tilde{F}_p$ =transmitted force matrix from the interface, $\tilde{F}_w$ =dynamic wind loading, $\tilde{F}_c$ =current loading on hull, and $\tilde{F}_{WD}$ =wave drift damping force matrix.

The static problem of the integrated system was solved using Newton's iterative method. The dynamic problem was integrated using an efficient and reliable time marching scheme similar to Adams-Moulton method (Garrett, 1982). In the dynamic program, special consideration is required due to the fact that the time derivatives of $\lambda$ do not appear in the equations and the added mass matrix is a function of the instantaneous position. In addition, the free-surface fluctuation and possible contact of mooring lines and catenary risers with the seafloor require special consideration.

## Results and Discussion

***Static Offset Test***

The static offset tests were first predicted by the vessel/mooring/riser coupled statics/dynamics program (WINPOST) for the mooring configurations of Figure 3. They are compared with test results and given in Figures 6 and 7. The computed prototype surge offset curves with its full-length moorings exhibit nonlinear weakening behavior. Whereas, the surge stiffness of the truncated mooring system with springs used in the OTRC experiments is almost linear. There is little difference between 12-line and equivalent 4-line results showing that the 4-line system can be used as a simpler model both in experiment and computation. Figure 7 shows that the taut-side line tension linearly increases with surge offset, while the slack-side line tension decreases in a non-monotonic manner.

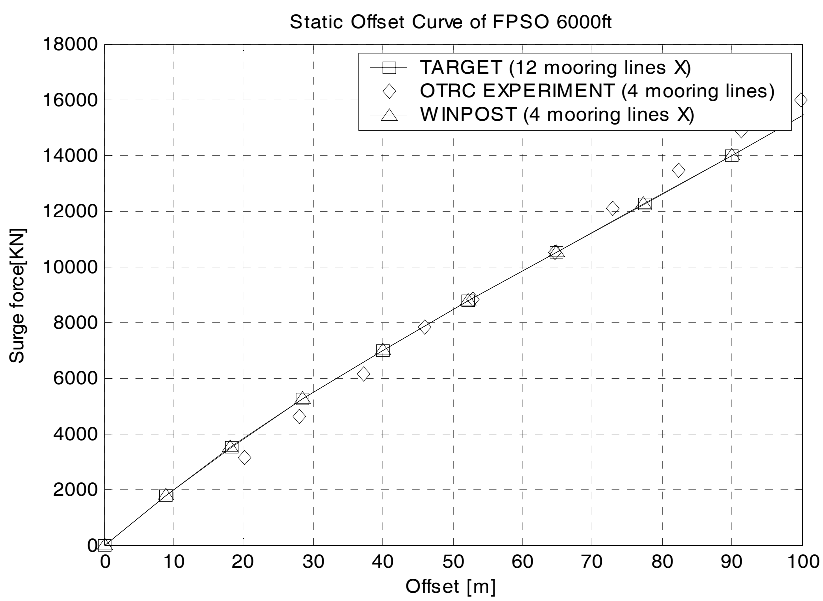


**Figure 6.** Comparison of the static offset test results.

Surge static offset curves obtained by OTRC experiment vs. WINPOST-FPSO simulation

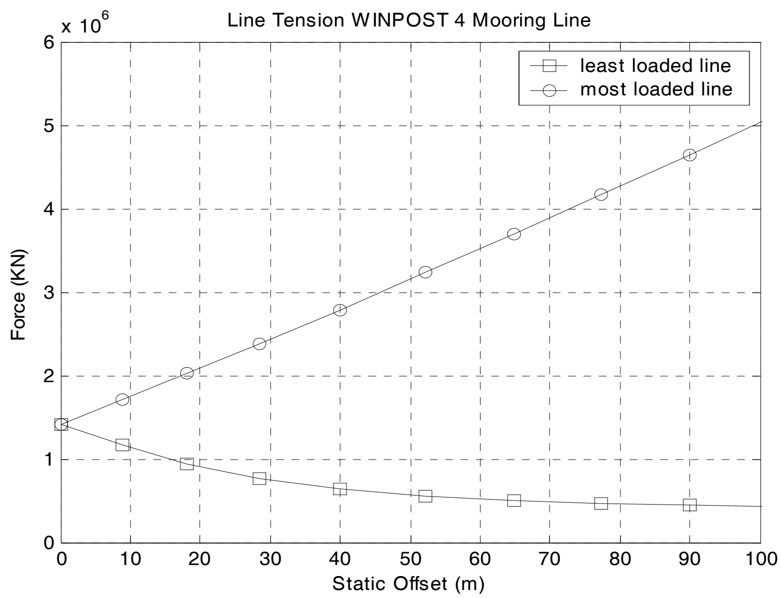


**Figure 7.** Comparison of the line tension in surge static offset test

### *Free Decay Test*

The total damping of the hull/mooring system can be obtained from the free decay tests. Simulations (4 X-shaped equivalent mooring lines in full length without riser) of the free decay tests are shown in Figure 8. The system's natural period and damping can be read from the free-decay time histories. The natural periods and damping coefficients are compared with the OTRC experiments (with truncated mooring system and spring) Table 5.

The comparisons of natural periods for various modes look satisfactory ensuring the proper numerical modeling of the real system. There exist some discrepancies in the predicted and measured values of damping ratios. The difference in roll damping is particularly noticeable due to the lack of viscous effects, which can be tuned by adding appropriate external damping in numerical modeling. Except for roll, the experimental damping is smaller than the numerical damping due to less contribution from truncated mooring system. The damping in general depends on motion amplitudes i.e. damping is larger in greater motion amplitudes. The first seven peaks were included for the estimation of Table 5.

**Table 5.** Comparison of the free decay test results

| | **OTRC EXPERIMENT** | | **WINPOST FPSO (4 mooring lines)** | |
|---|---|---|---|---|
| | **Periods (sec)** | **Damping Ratio (%)** | **Periods (sec)** | **Damping Ratio (%)** |
| **SURGE** | 206.8 | 3.0 | 204.7 | 4.4 |
| **HEAVE** | 10.7 | 6.7 | 10.8 | 11.8 |
| **ROLL** | 12.7 | 3.4 | 12.7 | 0.7 |
| **PITCH** | 10.5 | 8.0 | 10.8 | 10.5 |

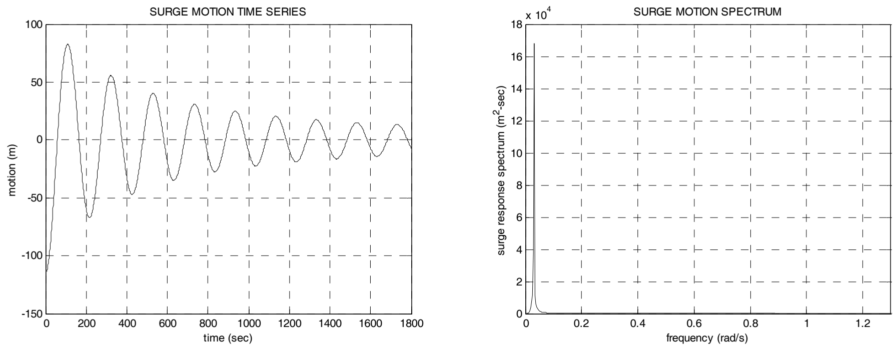


(a) Surge free decay simulation results

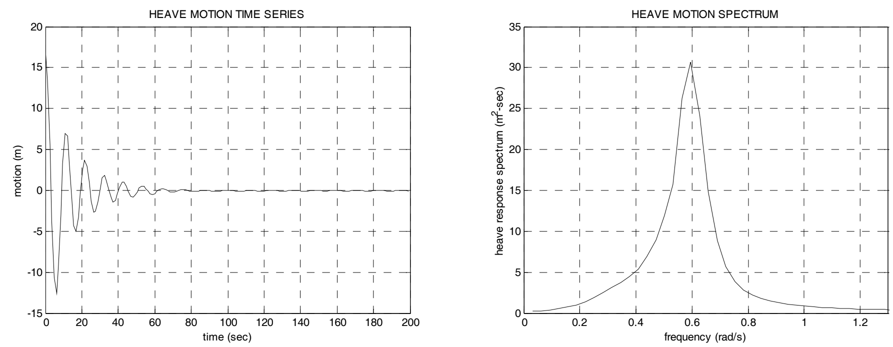


(b) Heave free decay simulation results

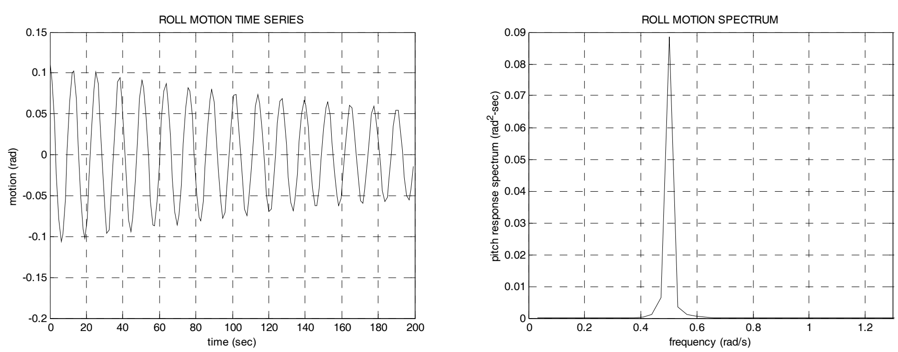


(c) Roll free decay simulation results

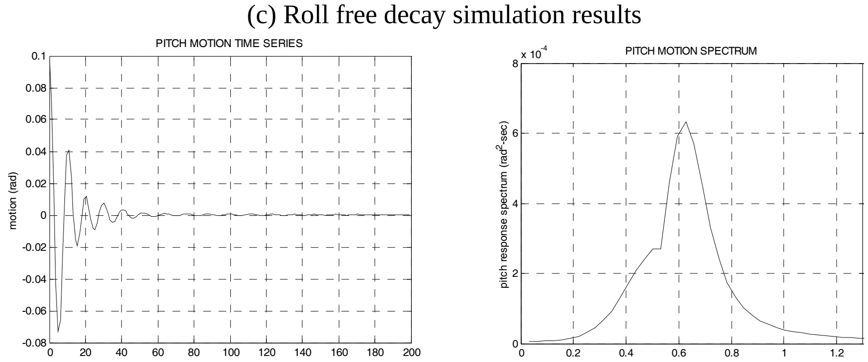


(d) Pitch free decay simulation results

**Figure 8.** Summary of free decay simulation results

***Time Simulation Results for 100-yr Nonparallel Hurricane*.**

The comparison of the OTRC experiment and the WINPOST-FPSO simulation is shown in Figure 9 and Table 6. The figures and table show that they are generally in good agreement. Low frequency slowly varying motions are dominant for horizontal plane modes (surge-sway-yaw), while wave frequency motions are pronounced for vertical plane modes (heave-roll-pitch). In Table 6, the low frequency (below 0.2 rad/s) standard deviation is separately given in addition to the wave-frequency component. The largest discrepancy between the prediction and measurement can be observed in roll motions, which is due to the pronounced role of viscous effects in that mode. It can be empirically tuned by adding proper roll viscous damping coefficient. Figure 10 shows hull drag coefficients proposed by Wichers (1998, 2001a and 2001b) for the same full-load FPSO. In the present numerical simulation with lighter loading condition, we use same drag coefficient as full-load FPSO, but the drag area is 90 % of full-load FPSO case.

The differences between the predicted and measured values can be attributed to many possible mismatches between numerical and physical models, such as truncated mooring system, uncertainty related to wind and current generation, etc. Despite the uncertainties, the correlation looks very reasonable.

The mean line tension of the truncated mooring system at the taut side is about 10% smaller, while that at the slack side is 30-40% larger when compared to the full-length system used in numerical analysis. The dynamic mooring top tension measured from OTRC experiments is about 20% smaller than that of numerical simulation with full-length mooring (see Table 7). The underestimation of dynamic mooring load is mainly caused by the mooring line truncation (distorted modeling) in the experiment due to the depth limitation of the OTRC wave basin. Even if the surge stiffness was artificially matched in the model testing by using clumps/buoys and springs, the dynamic similitude with truncated mooring system is very hard to achieve. In mooring tension spectra, it can be observed that slowly varying components are generally greater than wave-frequency components, and therefore, the mooring lines behave mostly in a quasi-static manner. It is why the discrepancy is not so large in this case. In the case of semi-taut mooring system, greater dynamic effects are expected (Kim et al, 2002), which may result in greater error in dynamic mooring tension measurement with truncated mooring system. The above argument can be clearly seen in the mooring-tension spectra of Figure 11, where the taut-side-mooring (#1,4) has negligible wave-frequency component, while the slack-side-mooring (#2,3) has appreciable wave-frequency component. Therefore, dynamic effects are less important in taut side. Due to the truncation of the mooring-line length, the wave-frequency tension components are under-estimated compared to the full-length case.

As for global vessel motions, the analysis results are reasonable compared to the experiments in view of overall trend. In the present simulations, the Newman's approximation scheme is used for evaluating the second-order difference-frequency wave forces and wave drift damping neglected, which was shown to be acceptable in Kim (2003).

Finally, the magnitudes of environmental loading components (wave, wind, current, and radiation damping forces and moments) for surge and sway are compared in Figure 12 and Table 8. It is seen that the mean loading by wind and current is greater than the mean wave drift force, while wave induced dynamic loading is greater than wind and current induced dynamic loading in the present case. The statistics of the environmental loadings are summarized in Table 8.

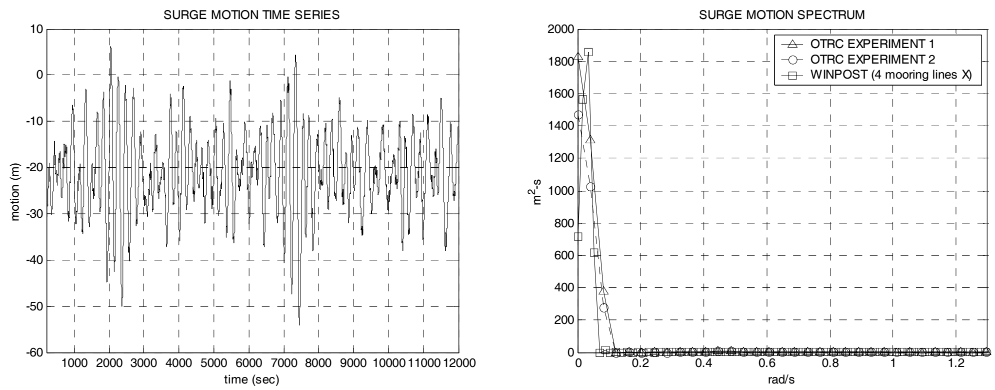


(a) Surge motion time series and spectrum

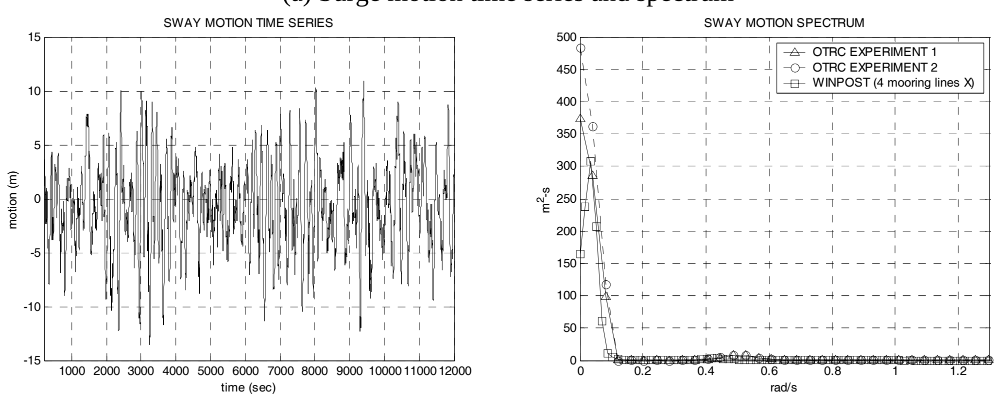


(b) Sway motion time series and spectrum

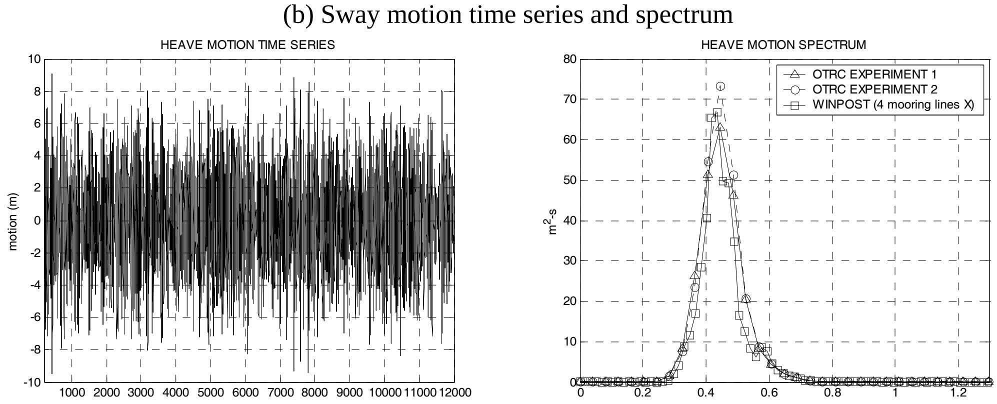


(c) Heave motion time series and spectrum

**Figure 9.** Summary of 100-year hurricane condition simulation results (4-mooring lines) (Continued)

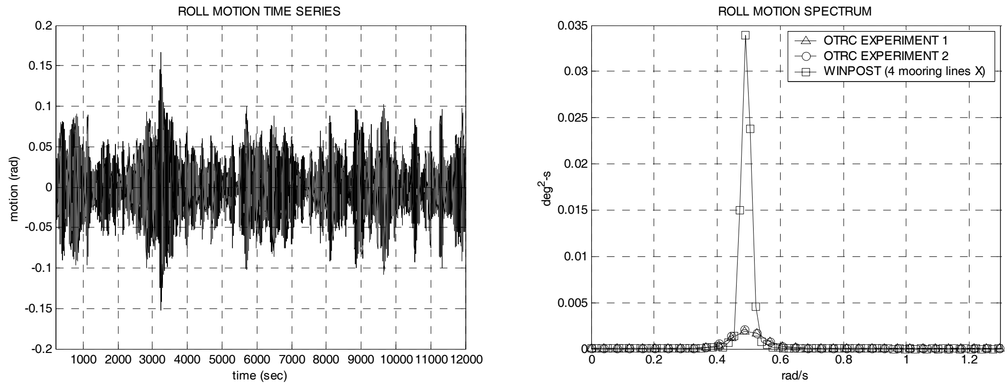


(d) Roll motion time series and spectrum

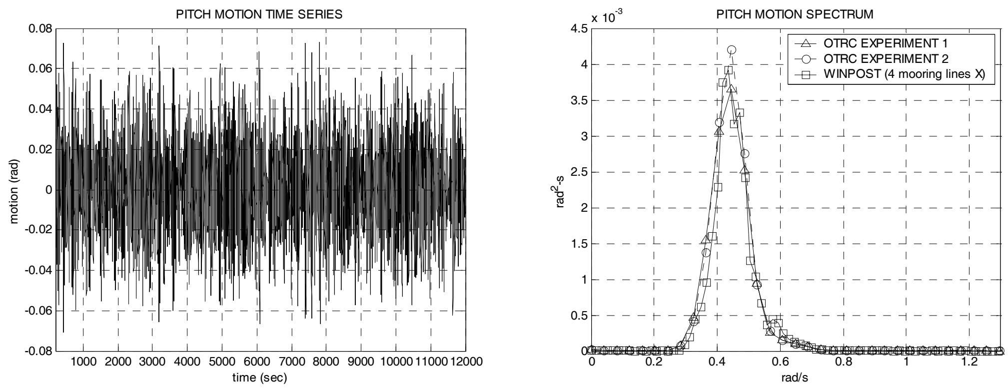


(e) Pitch motion time series and spectrum

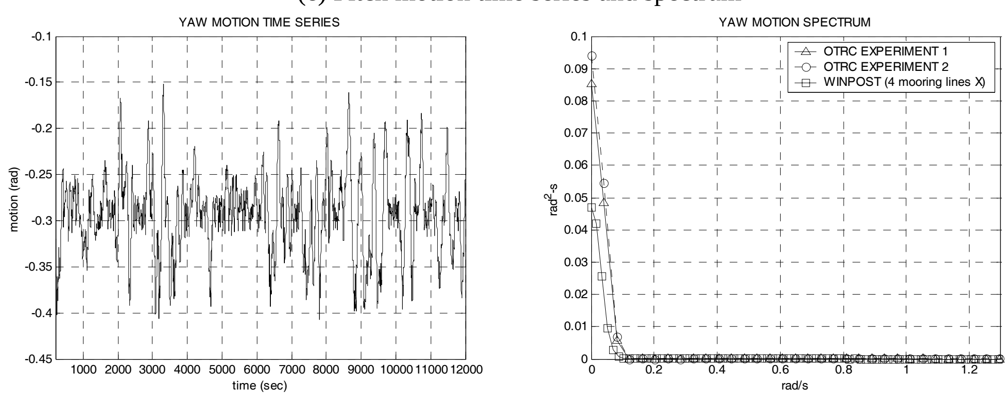


(f) Yaw motion time series and spectrum

**Figure 9.** Summary of 100-year hurricane condition simulation results (4-mooring lines)

**Table 6.** Comparison of the 100-year hurricane condition results

| | | OTRC Experiment | WINPOST - FPSO | |
|---|---|---|---|---|
| | | **4-mooring lines X-shape, truncated** | **4-mooring lines X-shape, full-length** | **12-mooring lines X-shape, full-length** |
| **SURGE (m)** | **MEAN** | -22.90 | -21.10 | -21.10 |
| | **MIN** | -61.30 | -54.10 | -55.00 |
| | **MAX** | 2.29 | 6.30 | 7.15 |
| | **STD** | 9.72 | 8.78 | 8.99 |
| | **WF STD** | N/A | 0.65 | 0.65 |
| | **LF STD** | N/A | 8.77 | 8.98 |
| **SWAY (m)** | **MEAN** | -0.09 | -0.64 | -0.54 |
| | **MIN** | -21.40 | -13.60 | -13.40 |
| | **MAX** | 13.10 | 10.90 | 10.30 |
| | **STD** | 4.57 | 4.05 | 3.89 |
| | **WF STD** | N/A | 0.61 | 0.61 |
| | **LF STD** | N/A | 4.00 | 3.84 |
| **HEAVE (m)** | **MEAN** | 0.14 | -0.06 | -0.06 |
| | **MIN** | -11.30 | -9.52 | -9.51 |
| | **MAX** | 10.90 | 9.11 | 9.11 |
| | **STD** | 3.08 | 2.81 | 2.81 |
| | **WF STD** | N/A | 2.81 | 2.81 |
| | **LF STD** | N/A | 0.03 | 0.03 |
| **ROLL (deg)** | **MEAN** | -0.10 | -0.08 | -0.08 |
| | **MIN** | -3.60 | -8.77 | -9.01 |
| | **MAX** | 3.50 | 9.57 | 9.85 |
| | **STD** | 0.90 | 2.18 | 2.19 |
| | **WF STD** | N/A | 2.17 | 2.18 |
| | **LF STD** | N/A | 0.12 | 0.12 |
| **PITCH (deg)** | **MEAN** | 0.01 | 0.03 | 0.03 |
| | **MIN** | -4.99 | -4.07 | -4.07 |
| | **MAX** | 4.45 | 4.20 | 4.20 |
| | **STD** | 1.31 | 1.26 | 1.26 |
| | **WF STD** | N/A | 1.26 | 1.26 |
| | **LF STD** | N/A | 0.02 | 0.02 |
| **YAW (deg)** | **MEAN** | -16.00 | -16.80 | -16.70 |
| | **MIN** | -24.60 | -23.30 | -23.40 |
| | **MAX** | -3.40 | -8.69 | -8.64 |
| | **STD** | 3.80 | 2.46 | 2.47 |
| | **WF STD** | N/A | 0.30 | 0.30 |
| | **LF STD** | N/A | 2.44 | 2.45 |

**Table 7.** Comparison of the mooring tension

| | | OTRC Experiment | WINPOST - FPSO | |
|---|---|---|---|---|
| | | **4-mooring lines X-shape, truncated** | **4-mooring lines X-shape, full-length** | **12-mooring lines X-shape, full-length** |
| **MOORING #1 (KN)** | **MEAN** | 5910 | 6470 | 6450 |
| | **MIN** | 3680 | 3100 | 3420 |
| | **MAX** | 10400 | 10700 | 10700 |
| | **STD** | 827 | 1080 | 1100 |
| **MOORING #2 (KN)** | **MEAN** | 3800 | 2760 | 2750 |
| | **MIN** | 1900 | 733 | 791 |
| | **MAX** | 6360 | 5340 | 5660 |
| | **STD** | 640 | 711 | 719 |
| **MOORING #3(KN)** | **MEAN** | 3430 | 2660 | 2670 |
| | **MIN** | 1410 | 529 | 532 |
| | **MAX** | 5560 | 5750 | 5480 |
| | **STD** | 587 | 722 | 726 |
| **MOORING #4(KN)** | **MEAN** | 5600 | 6320 | 6330 |
| | **MIN** | 2930 | 3450 | 3180 |
| | **MAX** | 8130 | 9710 | 9860 |
| | **STD** | 801 | 997 | 1010 |

Remarks: 1) Top tension = single line top tension X 3

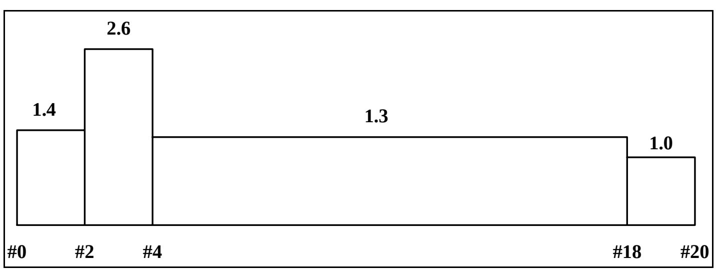


**Figure 10.** Hull drag coefficients proposed by Wichers (1998, 2001a and 2001b)

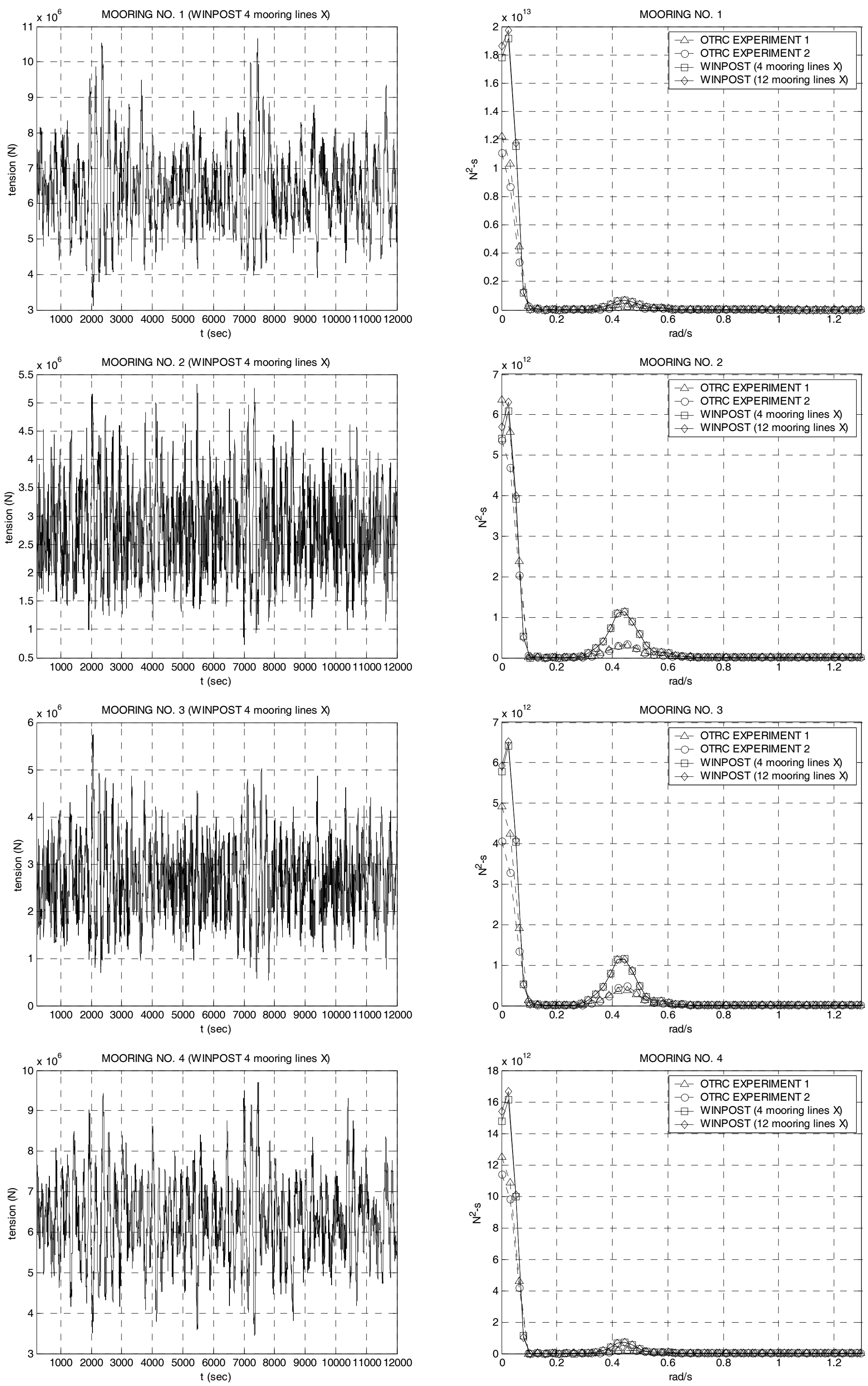


**Figure 11.** Summary of mooring line tension time series and spectra

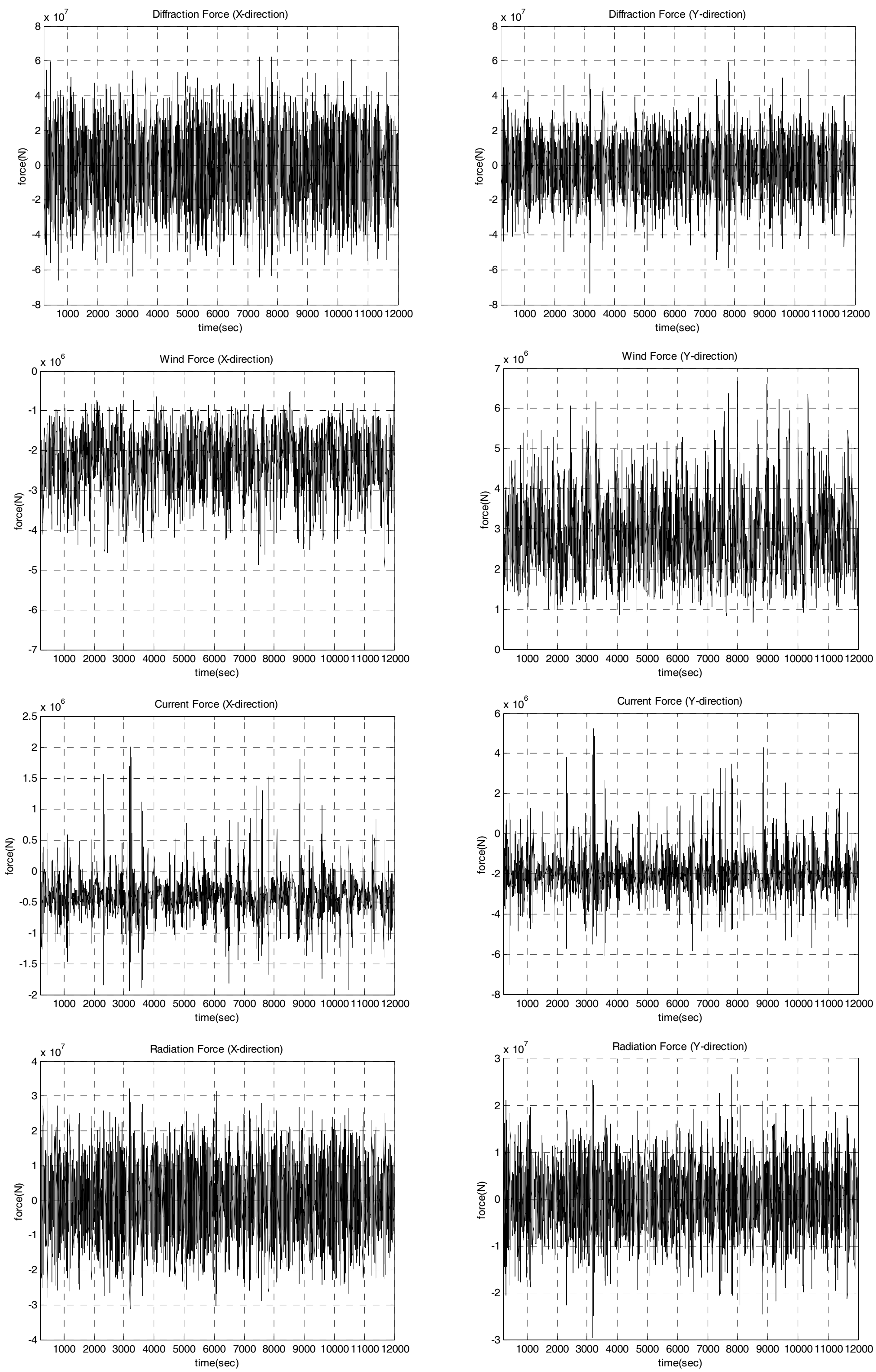


**Figure 12.** Summary of environmental loading component on FPSO

**Table 8.** Magnitudes of Computed Forces on FPSO

| | | SURGE (N) | SWAY (N) | HEAVE (N) | ROLL (N-m) | PITCH (N-m) | YAW (N-m) |
|---|---|---|---|---|---|---|---|
| **DIFFRACTION** | **MEAN** | -1.05E+06 | -8.69E+05 | 2.63E+06 | 2.03E+07 | 6.49E+08 | 7.40E+07 |
| | **STD** | 1.89E+07 | 1.38E+07 | 4.81E+07 | 5.00E+07 | 8.86E+09 | 2.97E+09 |
| **WIND** | **MEAN** | -2.26E+06 | 2.83E+06 | 0.00E+00 | -2.15E+07 | -1.70E+07 | -2.36E+08 |
| | **STD** | 6.48E+05 | 8.40E+05 | 0.00E+00 | 6.73E+06 | 4.86E+06 | 9.59E+07 |
| **CURRENT** | **MEAN** | -4.33E+05 | -1.99E+06 | 9.06E+03 | -1.55E+07 | 5.44E+06 | 1.58E+08 |
| | **STD** | 2.70E+05 | 8.24E+05 | 3.90E+04 | 8.23E+06 | 8.01E+06 | 1.77E+08 |
| **RADIATION** | **MEAN** | 1.02E+03 | -4.23E+03 | 8.78E+03 | 2.16E+03 | -3.71E+05 | 6.76E+03 |
| | **STD** | 9.61E+06 | 6.34E+06 | 2.83E+07 | 1.31E+07 | 5.91E+09 | 1.12E+09 |

## Summary and Conclusions

In the present study, the global motions and mooring dynamics of a deepwater (6000-ft) turret-moored FPSO in non-parallel 100-yr hurricane are numerically simulated and the numerical results are compared with the 1:60 model-testing results with truncated mooring system in the OTRC wave basin at Texas A&M University. The system's stiffness and line tension as well as natural periods/damping obtained from the numerically simulated static-offset and free-decay tests are in good agreement with the OTRC experimental results. The global vessel motion simulations in the hurricane condition were conducted by using the empirically suggested OCIMF and lateral-hull-drag coefficients. The agreement between the predicted and measured values is very good even without any extra effort for tuning and calibration. The noticeable discrepancy in FPSO roll motions is caused by viscous effects and it can further be reduced and tuned by using additional viscous-damping input in roll. The differences between measured and predicted results can be attributed to the uncertainties related to viscous effects, wind force generation, the current profile and unsteadiness, the mooring line truncation, and the usage of springs/buoys/clumps in truncated mooring lines. It is particularly underscored that the dynamic mooring tension can be underestimated with truncated mooring system when mooring dynamic effects are significant. The mooring line damping can also be significantly underestimated depending on the level of mooring-line truncation. The differences will be even more pronounced with additional risers and riser truncation.

## Acknowledgement

The present research is financially supported by the Offshore Technology Research Center (Industrial Consortia) and the Mineral Management Service. The assistance of OTRC basin staffs is also acknowledged.

## References

Arcandra, T. 2001. Hull/Mooring/Riser Coupled Dynamic Analysis of a Deepwater Floating Platform with Polyester Lines. Ph.D. Dissertation, Civil Engineering Department, Texas A&M University, College Station, TX.

Arcandra, T., Nurtjahyo, P. & Kim, M.H. 2002. Hull/Mooring/Riser Coupled Analysis of a Turret-Moored FPSO 6000 ft: Comparison between Polyester and Buoys-Steel Mooring Lines. Proc. 11th Offshore Symposium The Texas Section of the Society of Naval Architects and Marine Engineers, SNAME, 1-8.

Garrett, D.L. 1982. Dynamic Analysis of Slender Rods. J. of Energy Resources Technology, Trans. of ASME, 104, 302-307.

Kim, M.H., Arcandra, T. & Kim, Y.B. 2001a. Validability of Spar Motion Analysis against Various Design Methodologies/Parameters. Proc. 20th Offshore Mechanics and Arctic Eng. Conference, OMAE01-OFT1063 [CD-ROM], L.A., Califonia.

Kim, M.H., Arcandra, T. & Kim, Y.B. 2001b. Validability of TLP Motion Analysis against Various Design Methodologies/Parameters. Proc. 11th Int. Offshore and Polar Eng. Conference, ISOPE, 3, 465-473.

Kim, M.H., Ran, Z., and Zheng, W. 2001. Hull/mooring coupled dynamic analysis of a truss spar in time domain. Int. Journal of Offshore and Polar Engineering, Vol.11, No.1, 42-54.

Kim, Y.B. and Kim, M.H. 2002. Hull/Mooring/Riser Coupled Dynamic Analysis of a Tanker-Based Turret-Moored FPSO in Deep Water. Proc. 12th Int. Offshore and Polar Eng. Conference, ISOPE, Vol.1, 169-173.

Kim, Y.B. 2003. Dynamic Analysis of Multiple-Body Floating Platforms Coupled with Mooring Lines and Risers. Ph.D. Dissertation, Civil Engineering Department, Texas A&M University, College Station, TX.

Lee, C.H. 1999. WAMIT User Manual. Dept. of Ocean Engineering, Massachusetts Institute of Technology, Cambridge, M.A.

Lee, D.H. and Choi, H.S. 2000. A dynamic analysis of FPSO-shuttle tanker system. Proc. 10th Int. Offshore and Polar Eng. Conference, ISOPE, Vol.1, 302-307.

Ma, W., Lee, M.Y., Zou, J. & Huang, E. 2000. Deep Water Nonlinear Coupled Analysis Tool. Proc. Offshore Technology Conference, OTC 12085 [CD-ROM], Houston, Texas.

OCIMF. 1994. Prediction of Wind and Current Loads on VLCCs. 2nd Edition, Witherby & Co. Ltd, London, England.

Ran, Z. and Kim, M.H. 1997. Nonlinear coupled responses of a tethered spar platform in waves. Int. Journal of Offshore and Polar Engineering, Vol. 7, No. 2, pp. 111-118.

Ran, Z. 2000. Coupled Dynamic Analysis of Floating Structures in Wave and Current. Ph.D. Dissertation, Civil Engineering Department, Texas A&M University, College Station, TX.

Sphaier, S.H., Fernandes,A.C., and Correa,S.H. 2000. Maneuvering model for the FPSO horizontal plane behavior. Proc. 10th Int. Offshore and Polar Eng. Conference, ISOPE, Vol.1, 337-344

Ward, E.G., Irani, M.B. and Johnson, R.P. 2001. The Behavior of a Tanker-Based FPSO in Hurricane Waves, Winds, and Currents. Proc. 11th Int. Offshore and Polar Eng. Conference, ISOPE, 4, 650-653.

Ward, E.G., Kim, M. H., Hansen, V.L. and Wang, L. 2004. DeepStar Theme Structure Studies. Proc. Offshore Technology Conference, OTC 16586 [CD-ROM], Houston, Texas.

Wichers, J.E.W. 1988. A Simulation Model for a Single Point Moored Tanker. Ph.D. Dissertation, Delft University of Technology, Delft, The Netherlands.

Wichers, J.E.W. & Develin, P.V. 2001a. Effect of Coupling of Mooring Lines and Risers on the Design Values for a Turret Moored FPSO in Deep Water of the Gulf of Mexico. Proc. 11th Int. Offshore and Polar Eng. Conference, ISOPE, 3, 480-487.

Wichers, J.E.W, Voogt, H.J., Roelofs, H.W. & Driessen, P.C.M. 2001b. DeepStar-CTR 4401- Benchmark Model Test. Technical Rep. No. 16417-1-OB, MARIN, Wageningen, Netherlands.

Wichers, J.E.W., Devilin, P.V., 2004 Benchmark Model Tests on the DeepStar Theme Structures FPSO, SPAR, and TLP. Proc. Offshore Technology Conference, OTC 16582 [CD-ROM], Houston, Texas.